Mesoscale Indexing of the Distribution of Orographic Precipitation over High Mountains

P. ALPERT

Dept. of Geophysics and Planetary Sciences, Raymond and Beverly Sackler Faculty of Exact Sciences, Tel Aviv University, Israel

(Manuscript received 1 June 1985, in final form 28 September 1985)

ABSTRACT

A simple analytical expression for indexing the orographic precipitation rate over high mountains is presented. The formula is based upon the assumption that the moisture convergence in the mountainous boundary layer approximately equals the precipitation. Realistic precipitation distributions are obtained when numerical advection is permitted for the Himalayas, Equadorian Andes and the Sierra Nevada Mountains in California. In the latter case the simulated distributions compete well with a fully two-dimensional precipitation model for some unusual stormy events. Following the model results over high mountains, it is suggested that for the distribution of precipitation, particularly over the high mountains, the detailed microphysical processes may play a lesser essential role than that for small to medium size mountains.

The elevation of maximum orographic precipitation, z_m, is investigated and an analytical expression for z_m is derived for a bell-shaped mountain. This expression predicts z_m values that are in general agreement with observations. The elevation of maximum precipitation z_m is found to always be shifted to lower levels than the point of the steepest slope. It is also shown that an upper limit for z_m exists. This upper limit is independent of the mountain height and is determined mainly by the moisture scale height and the tropospheric scale height.

In addition to the two maxima of precipitation over the Himalayas that have been observed in the foothills and at about 2–2.4 km, a third unknown maxima is predicted by the theory. This unobserved maxima is predicted over the Great Himalayan Range at the height of 4 km. Such a maxima, if it exists, could not be detected due to the lack of enough observations at high elevations.

1. Introduction

The distribution of rainfall over mountains has important applications for agriculture and hydrology. It becomes evident from the observations that the elevation of any point on a mountain strongly affects the amount of precipitation at that point. Earlier studies searched a linear relationship between elevation and precipitation. Such studies have been carried out by Donley and Mitchell (1939) in the Southern Appalachian region of the United States, Stidd and Leopold (1951) in Hawaii, Rodda (1962) in England and Rumley (1965) in the Equadorian Andes. One can say that the correlation coefficient between elevation and precipitation was generally found to be low, for example, 0.24 for the Andes (Rumley, 1965), 0.19 for the Himalayas (Dhar and Rakhecha, 1980) and 0.30 for Western Colorado (Linsley et al., 1958). This low correlation was not unexpected because there are additional important factors like slope, orientation and large-scale effects. In fact, one should expect maximum precipitation at some elevation, as explained by Burns (1953). The maximum is the combined result of two opposing effects; one is due to the enhanced moisture condensation as the barrier height increases and the other is due to the exponential reduction in the quantity of available moisture with increasing elevation.

Spreen (1947) studied the orographic influences upon seasonal precipitation by defining five topographic factors: elevation, slope, rise, orientation and exposure. He was able to show that in western Colorado the five parameters together accounted for 85 percent of the precipitation while elevation alone accounted for only about 30 percent of the variation in the precipitation. Similar results were found by Burns (1953) in discussing the small-scale topographic effects in the San Gabriel Mountains in California.

In this study, we shall concentrate on the mesoscale indexing of the distribution of orographic precipitation rates. The detailed air flow over the mountain and the cloud microphysics are not included in our model, but the precipitation rate estimates are based on the assumption that orographic precipitation approximately equals the convergence of moisture in the mountainous boundary layer. Results are compared with some intense rainfall case studies from Colton (1976).

Special attention is given to the elevation of maximum precipitation and the factors that determine this height. The elevation of maximum precipitation is about 1 km in the western Andes of Equador (see Rumley, 1965), but between 1 and 2 km in the Sierra Nevada Mountains in California. At the central Himalayas, Dhar and Rakhecha (1980) show that the elevation and rainfall can best be related by a fourth-degree polynomial and that the rainfall elevation profiles show two zones of maximum rainfall, one near the foothills and the other at an elevation of 2.0 to 2.4 km. In section 3 the aforementioned distributions are

discussed in light of the theory presented in section 2. The possible existence of a third maxima over the Great Himalayan Range (at ~4 km) is also described.

2. Theory

a. Basic equation

From tropical observations by Cho and Ogura (1974) there is an approximate equality between vertical moisture flux through deep clouds and low-level moisture convergence. This was found also during GATE (1980), and Stevens and Lindzen (1978) adopted such a relation for the study of the tropical Wave-CISK. The precipitation rate could then be well approximated by

$$P = -\int_0^{H_0} \nabla_H \cdot (\rho q \mathbf{V}) dz + E, \tag{1}$$

where P and E represent precipitation rate and evaporation for a column with unit horizontal area, H_0 is the top of the moist layer, q and $\mathbf{V}$ are specific humidity and horizontal velocity. The equality expressed by (1) assumes that no storage of moisture occurs and this is not always true. On substitution from the approximate continuity equation

$$\nabla_H \cdot (\rho \mathbf{V}) = -\partial(\rho W)/\partial z, \tag{2}$$

one obtains

$$P = -\bar{q} \int_0^{H_0} -\frac{\partial(\rho W)}{\partial z} dz + E$$

$$\approx \bar{\rho}\bar{q}[-(\overline{\nabla_H \cdot \mathbf{V}})H_0] + E, \tag{3}$$

where $\bar{q}$, $\bar{\rho}$ are the vertically averaged specific humidity and air density for the moist layer, and $-(\overline{\nabla_H \cdot \mathbf{V}})H_0$ is the total convergence into the column up to its top H_0, i.e.,

$$-\int_0^{H_0} \nabla_H \cdot \mathbf{V} dz.$$

The total convergence is then decomposed into that ascribed to the orographic effect and that to large-scale causes. For estimation purposes, the column integral is evaluated first from the mountain surface to mountaintop level (designated δz). This integral yields in two dimensions (x, z), a velocity convergence of $u(\partial Z_s/\partial x)$, where Z_s represents the terrain contours. This is illustrated in the dimensions (x, z) as

$$-\int_0^{\delta z} \frac{\partial u}{\partial x} dz \approx -\frac{\delta u}{\delta x} \cdot \delta z = u \frac{\delta z}{\delta x} = \mathbf{V} \cdot \nabla Z_s,$$

where u is the horizontal speed and δz is the elevation of the horizontal surface at mountaintop. This horizontal convergence due to topography is referred to (particularly in large-scale dynamics) as the lower boundary condition for the *vertical* velocity, which is expressed through the continuity equation as follows:

$$W(0) = \mathbf{V}_s \cdot \nabla Z_s,$$

e.g., see Haltiner and Williams (1980, p. 209). The upper integral is the contribution of horizontal convergence that might well be the result of large-scale dynamics and will therefore be denoted by W_l. Consequently,

$$-\int_0^{H_0} (\nabla_H \cdot \mathbf{V}) dz = -(\overline{\nabla_H \cdot \mathbf{V}})H_0 = -\int_0^{\delta z} (\nabla_H \cdot \mathbf{V}) dz$$

$$-\int_{\delta z}^{H_0} (\nabla_H \cdot \mathbf{V}) dz = \mathbf{V} \cdot \nabla Z_s + W_l \tag{4}$$

where W_l is the large-scale (synoptic) contribution to the vertical velocity. On substitution of (4) into (3) one gets

$$P \approx \bar{\rho}\bar{q}(\mathbf{V} \cdot \nabla Z_s + W_l) + E. \tag{5}$$

Later we will assume for simplicity mountain uniformity in the y direction, or $u\partial Z_s/\partial x$ will replace $\mathbf{V} \cdot \nabla Z_s$, and a constant synoptically induced vertical velocity, W_l. We presume that the latter assumption cannot be easily justified as the large-scale systems and their induced vertical velocities are probably modified by the mountain. But the typical horizontal scale for such modifications is in general larger than that associated with the mesoscale effect of the mountain slope, and only this smaller scale effect is of our interest in this study. Another implicit assumption in (5) is that a similar moist layer depth can be taken for the whole mountainous region which is being considered. It will be shown that the contribution due to evaporation is relatively small. If u is assumed constant one gets from (5) that two main factors determine the distribution of precipitation over the mountain: the uplift induced by the local slope, and the decrease of moisture availability, ρq, with height. Although this precipitation formula is highly simplified, one may consider it for indexing the geographic distribution of the precipitation of a given mountainous region as it will later be illustrated. Furthermore, as (5) does not contain any advective effects, we adopt a summation procedure that simulates moisture advection. Examples of such summation are given in section 3, where simulated results are compared with real observations.

b. The elevation of maximum precipitation

One of the most interesting questions with regard to orographic precipitation is the height of the mountain at which the maximum precipitation occurs. It was well known that such a maximum exists for high mountains, and the physical causes for this were well explained by Burns (1953). Points of maximum precipitation were reported by Dhar and Rakhecha (1980, p. 260) at an elevation of 2.0 to 2.4 km for the monsoon precipitation at the Himalayas, by Rumley (1965, p. 61) at an elevation of about 1.0 km for the mean annual rainfall at the western slopes of the Andes, by Colton (1976) at the elevation ranging from 1.0 to 2.0 km for some case studies (typically for periods of a day or two)

at the Sierra Nevada Mountains. Linsley et al. (1949) report the height of 1.5 km for the maximum mean annual rainfall over the Sierra Nevada Mountains. The exact elevation of the maximum precipitation seems to be of special importance in hydrological studies. Of course, one should be aware of the fact that although orographic precipitation is generally the predominant type in mountainous terrain, it happens that due to effects of convection and some dry-layer presence the maximum precipitation may differ somewhat from the maximum precipitation rate that is being estimated by the present model. We shall now derive an analytical expression to estimate the elevation of maximum precipitation. Equation (5) could be rewritten as

$$P = \epsilon r e_s(Z_s)\left[\bar{u}\frac{\partial Z_s}{\partial x} + W_l\right]\Big/[RT(Z_s)] + C(1-r)\bar{u}e_s(Z_s)/L, \quad (6)$$

where we have substituted the following relations:

$$\left.\begin{aligned} q &\approx \epsilon e_a/p, \quad \text{where} \quad \epsilon \approx 0.622 \\ \rho &= p/RT \\ E &= C(e_s - e_a)\bar{u}/L \\ r &= e_a/e_s \end{aligned}\right\}. \quad (7)$$

The expressions e_a and e_s are the air vapor pressure and the saturated surface vapor pressure, respectively; C is an empirical constant,[1] R is the gas constant for dry air, and p is the air pressure. The variability of the gas constant with moisture in (7) was ignored, as it could be shown to be of the order of less than 5–10 percent. The saturated surface vapor pressure e_s may be expressed in terms of temperature at the elevation Z_s using the Clausius-Clapeyron equation (see e.g., Hess, 1959),

$$e_s(Z_s) \approx e_s(0)\exp\left[\frac{m_v L_c}{R^* T(0)}\frac{T(Z_s) - T(0)}{T(Z_s)}\right]. \quad (8)$$

Here, $e_s(0)$ is the saturated surface vapor pressure in temperature $T(0)$, m_v is the molecular weight of water, L_c is the latent heat of condensation, and R^* the universal gas constant. In order to find the elevation of maximum precipitation, (6) is differentiated with respect to x [$Z_s(x)$ represents mountain shape], and set equal to zero. On the assumption that $T(Z_s)$ decreases with elevation by a constant lapse-rate Γ one gets

$$(K_1/T)\frac{\partial^2 Z_s}{\partial x^2} + [aK_2 + K_3(a/T + \Gamma/T^2)]\frac{\partial Z_s}{\partial x} + K_1(a/T + \Gamma/T^2)\left(\frac{\partial Z_s}{\partial x}\right)^2 \approx 0, \quad (9)$$

where

$$\left.\begin{aligned} a &= -(L_c\Gamma)/(R_v T(0)T) \approx -(L_c\Gamma)/(R_v T^2(0)) \\ T &= T(Z_s) \\ R_v &= R^*/m_v. \end{aligned}\right\} \quad (10)$$

The three constants K_1, K_2 and K_3 represent the contributions due to the slope-induced uplift, evaporation, and large-scale uplift respectively and are given by

$$\left.\begin{aligned} K_1 &= \epsilon r\bar{u}e_s(0)/R \\ K_2 &= C(1-r)\bar{u}e_s(0)/L \\ K_3 &= \epsilon r W_l e_s(0)/R \end{aligned}\right\}. \quad (11)$$

The latent heat of condensation L and the relative humidity r were taken to be independent of height. To estimate the contribution due to evaporation relative to the "synoptic" contribution, we calculate the ratio η of $[K_3(a/T)]$ to $[a \cdot K_2]$ to be [see (9)]:

$$\eta = \frac{r}{(1-r)}\frac{W_l}{\bar{u}}\cdot\frac{L}{CRT} \approx 1.2 \times 10^3 \frac{W_l}{\bar{u}}\cdot\frac{r}{(1-r)}\epsilon. \quad (12)$$

It is reasonable to assume that the ratio of the large-scale uplift velocity to the horizontal wind impinging on the mountain, i.e., $W_l/\bar{u}$ is of the order of 10^{-2} -10^{-3}. Therefore, $\eta \gg 1$ if the air is not too dry (i.e., relative humidity $r > 0.85$). This assumption is a fairly good one in mountainous regions, particularly during periods of rain. Thus, the evaporation contribution to the precipitation will be neglected. This is equivalent to the assumption $r = 1$ or $K_2 = 0$. The large-scale contribution represented by the vertical velocity W_l or equivalently by K_3 will be shown later to have only a secondary effect. Taking $K_3 = 0$ and $K_2 = 0$, (9) reduces to

$$Q\left(\frac{\partial Z_s}{\partial x}\right)^2 = -\frac{\partial^2 Z_s}{\partial x^2}, \quad (13)$$

where

$$Q = a + \Gamma/T \approx \{1 - L_c/[R_v T(0)]\}\Gamma/T. \quad (14)$$

For $T(0) = 300$ K,

$$Q \approx -17\Gamma/T \approx -0.06\Gamma. \quad (15)$$

Equation (13) defines an elevation for which we might expect the maximum precipitation.

c. *An example: A bell-shaped mountain*

In order to assess the implication of the aforementioned relation, let us assume a bell-shaped mountain with a height H and half-width b, i.e.,

$$Z_s(x) = Hb^2/(x^2 + b^2). \quad (16)$$

[1] See for example, Ramage et al. (1972), who have used $C = 5.17$ (cal cm^{-2} d^{-1})/(mb m s^{-1}).

The substitution of (16) into (13) results in a fourth-order equation for x_m—the x value for which maximum precipitation is obtained—as follows.

$$3x_m^4 + 2b^2(1 + QH)x_m^2 - b^4 = 0. \quad (17)$$

By assuming that Q is approximately constant [see (15)] the solution is given by

$$x_m = \pm \frac{b}{\sqrt{3}} F, \quad (18a)$$

$$z_m = 3H/(F^2 + 3), \quad (18b)$$

and

$$F = [(4 + 2QH + Q^2H^2)^{1/2} - (1 + QH)]^{1/2}. \quad (18c)$$

In the unrealistic case of $Q \approx 0$, i.e., an isothermic atmosphere ($\Gamma \approx 0$), one gets $F = 1$, yielding $(x_m, z_m) = (b/\sqrt{3}, 0.75H)$. The latter point is exactly where the bell-shaped mountain gets its maximum slope. This result is not unexpected, since the precipitation was assumed to be proportional to the slope of the mountain, and in this case the atmosphere is isothermic and saturated at all levels ($r = 1$). As the lapse rate increases or as the top height of the bell-shaped mountain, H, increases $QH \approx -0.06\Gamma \cdot H$ yields an F-value larger than 1. For example, if $\Gamma = \Gamma_s$ the saturated lapse rate, and $H = 5$ km, one gets from (15) that

$$QH \approx -0.06\Gamma_s H \approx -1.95;$$

$$\Gamma_s \approx 6.5°\text{C km}^{-1} \text{ (for } p = 1000 \text{ mb and } T = 0°\text{C)},$$

and from (18c), (18b) $F \sim 1.71$ yielding an elevation of 2.53 km for the maximum precipitation. Table 1 lists the elevations for which maximum precipitation is attained for a bell-shaped mountain of $H = 5$ km and $b = 100\sqrt{3}$ km (values that fit the Himalayas). For the exact derivation according to the real shape of the mountain see the next section. The values of x_m and z_m are calculated for some values of Γ_s ranging between 0 and $\Gamma_d = g/C_p$—the dry adiabatic lapse rate—where C_p is the specific heat of dry air at constant pressure, and g is the gravity acceleration.

We conclude that the maximum precipitation is obtained not above the steepest slope but rather shifted toward lower elevations. This shift becomes larger as $|-QH|$ increases. The reason for this is the following: as Γ increases the availability of moisture decreases rapidly with elevation, and consequently the elevation of maximum precipitation goes down. The increase of the mountain height has a similar effect above the horizontal shift if we keep Γ constant. Here, the higher the mountain is, the higher the point where the maximum is obtained, but if the mountain's aspect ratio H/b is kept constant, the elevation of maximum precipitation remains at the same point and the horizontal shift x_m is changing accordingly. Figure 1 shows the change of the normalized precipitation with height in the above example for three values of Γ, $\Gamma = 2$, 6.5 and 10°C km^{-1}. These results illustrate how the elevation of maximum precipitation, z_m, and the amounts of precipitation are strongly reduced as the lapse rate Γ increases. The predicted elevation of 2.5 km for the maximum precipitation in the above example is in general agreement with the result of Dhar and Rakhecha (1980), which is 2.0–2.4 km at the Himalayas. The values of $H = 5$ km, $b = 100\sqrt{3}$ km (in the table) and $\Gamma = 6.5°\text{C km}^{-1}$ were chosen to fit the Himalayan data in the above study. Similar results would apply to the Sierra Nevada and the Andes.

Another interesting question one may ask is whether there is an upper limit to z_m (elevation of maximum precipitation) as the mountain height increases indefinitely, and if it exists, what determines such a limit. On substituting (18c) into (18b) and taking the limit $H \to \infty$ one obtains

$$\max(z_m) = 3H/(F^2 + 3) \xrightarrow[H\to\infty]{} -1.5/Q. \quad (19)$$

Referring to (14), Q is estimated by

$$Q \approx -\frac{L_c}{R_v T(0)} \cdot \frac{\Gamma}{T}, \quad (20)$$

which on substitution to (19) yields

$$\max(z_m) = \frac{1.5R_v T(0)}{\Gamma} \cdot \frac{T}{L_c}. \quad (21)$$

If we let $T = \bar{T} \approx 270$ K then:

$$\max(z_m) = \begin{cases} \infty, & \Gamma = 0 \\ 1.5h \dfrac{m_d}{m_v} \dfrac{C_p}{L_c} \bar{T} \sim 2.3 \text{ km}, & \Gamma = \Gamma_d = g/C_p \\ \sim 3.8 \text{ km}, & \Gamma = \Gamma_s \sim 6.5°\text{C km}^{-1} \end{cases} \quad (22)$$

TABLE 1. The points (x_m, z_m) for which the maximum precipitation is obtained for a bell-shaped mountain of $H = 5$ km and $b = 100\sqrt{3}$ km.

	Γ (°C km^{-1})							
	0	1.3	2.6	3.9	5.2	6.5	7.8	9.8
$-QH$	0	0.39	0.78	1.17	1.56	1.95	2.34	2.94
F	1	1.11	1.24	1.38	1.54	1.71	1.88	2.13
x_m (km)	100	111	124	138	154	171	188	213
z_m (km)	3.75	3.6	3.3	3.1	2.8	2.5	2.3	1.98

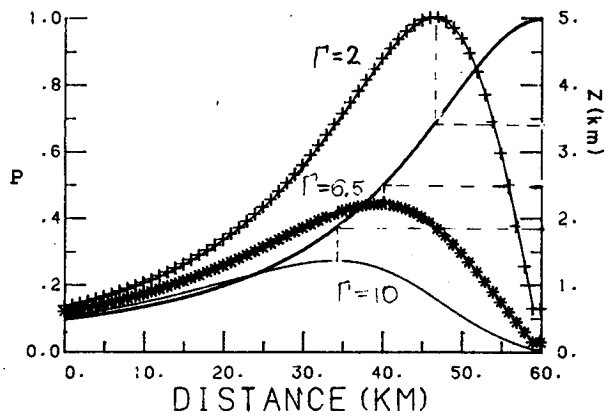

FIG. 1. The predicted normalized precipitation rates for three lapse rates: Γ = 2, 6.5 and 10°C km^{-1} plotted with crosses, asterisks and a solid curve, respectively. The heavy solid curve is the bell-shaped mountain with the height H = 5 km and half-width b = 20 km. The rates of precipitation are normalized by the maximum precipitation with Γ = 2°C km^{-1}.

where $h = RT(0)/g$ is the scale height of the atmosphere and m_d is the molecular weight of dry air. Equation (22) presents an upper limit of about 3.8 km to the elevation of the maximum precipitation for realistic lapse rates, regardless of mountain height or slope. Clearly this upper limit is a direct consequence of the severe reduction with height of the moisture availability, due to the cooling of the air, as expressed by the Clausius-Clapeyron equation. Figure 2 illustrates the upper limit for z_m which is independent of the mountain height or of its slopes and is solely a function of the atmospheric lapse rate. For example, for Γ = 6.5°C km^{-1} and H = 50 km, z_m reaches the value of 3.58 km.

In the foregoing discussion it was assumed that the relative humidity is constant with height and the reduction in the absolute humidity with height is due to the cooler air aloft. However, vertical profiles of humidity at the tropics indicate a nearly constant specific humidity $\bar{q}(0)$ through the boundary layer up to the level of the trade inversion H_0, above which it decreases very rapidly with height to a small value (e.g., see Augstein et al., 1974).

Therefore, let us assume that,

$$q = \begin{cases} q(0), & Z_s < H_0 \\ [q(0) - \Gamma_q(Z_s - H_0)], & Z_s > H_0 \end{cases} \quad (23)$$

and that the density is determined by the constant lapse rate Γ (as in the polytropic atmosphere), i.e.,

$$\rho = \rho(0)[T/T(0)]^{(g/\Gamma R)-1}. \quad (24)$$

Here we have tacitly assumed that the moisture structure over the tropical mountains is basically the same as over the ocean and the leveled terrain. The lapse rates Γ and Γ_q stand for the temperature lapse-rate and for the specific humidity lapse-rate (above the inversion), respectively.

On substitution of (23) and (24) into (5), differentiating with respect to x and again assuming that $W_l = 0$, $E = 0$; one obtains (13) for the point of the maximum precipitation except with a different Q, i.e.,

$$Q = -\frac{g}{RT} + \frac{\Gamma}{T} - \frac{\Gamma_q}{q} = -\frac{1}{h} + \frac{1}{h_T} - \frac{1}{h_q}. \quad (25)$$

In this case max(z_m) for the bell-shaped high mountains ($H \to \infty$) following (19) yields,

$$\max(z_m) = 1.5 \Big/ \left(\frac{1}{h} - \frac{1}{h_T} + \frac{1}{h_q}\right), \quad (26)$$

where h, h_T and h_q represent tropospheric scale height (RT/g), temperature scale height, $T(0)/\Gamma$, and moisture scale height, $\sim q(0)/\Gamma_q$, respectively. Of course, the smallest scale height in (26) will determine the height of the maximum precipitation. A typical value for h is about 8 km and for $h_T \sim$ 40–50 km while h_q in the tropics is relatively small and may be estimated, following Augstein et al. (1974) as 3–5 km. Taking,

$$h_q < h \ll h_T; \quad h \approx 2h_q \Rightarrow \max(z_m) = h_q \sim 4 \text{ km}. \quad (27)$$

In the extreme case where $\Gamma_q \sim 0$ or $h_q \to \infty$, i.e., the specific humidity is constant through the atmosphere, one obtains

$$h \ll h_T \ll h_q \Rightarrow \max(z_m) \approx 1.5h \sim 12 \text{ km}. \quad (28)$$

Thus, in quite realistic moisture structures of the tropics there is an upper limit for the elevation of maximum precipitation given by the moisture scale height of the troposphere. But, if there is no reduction of the specific humidity with height, the tropospheric scale height bounds z_m.

d. The effect of large-scale uplift (W_l)

In deriving (13) for the point of maximum precipitation, it was assumed for reasons of simplicity that the synoptic or large-scale contribution to the vertical velocity, W_l, may be neglected. Taking nonzero constant W_l leads to $K_3 \neq 0$ and (9) becomes

$$\frac{\partial^2 Z_s}{\partial x^2} + \left(\frac{K_3}{K_1} Q\right)\frac{\partial Z_s}{\partial x} = -Q\left(\frac{\partial Z_s}{\partial x}\right)^2. \quad (29)$$

The second term on the left of (29) is new as compared to (13). From (11),

$$\frac{K_3}{K_1} Q = \frac{W_l}{\bar{u}} Q = \delta Q, \quad (30)$$

where $\delta = W_l/\bar{u} \approx 10^{-2}$–$10^{-3}$. For the bell-shaped mountain, (29) yields for the point x_m,

$$-\delta Q x_m^5 + 3x_m^4 - 2\delta Q x_m^3 + 2b^2(1 + QH)x_m^2 - \delta Q b^4 x_m - b^4 = 0, \quad (31)$$

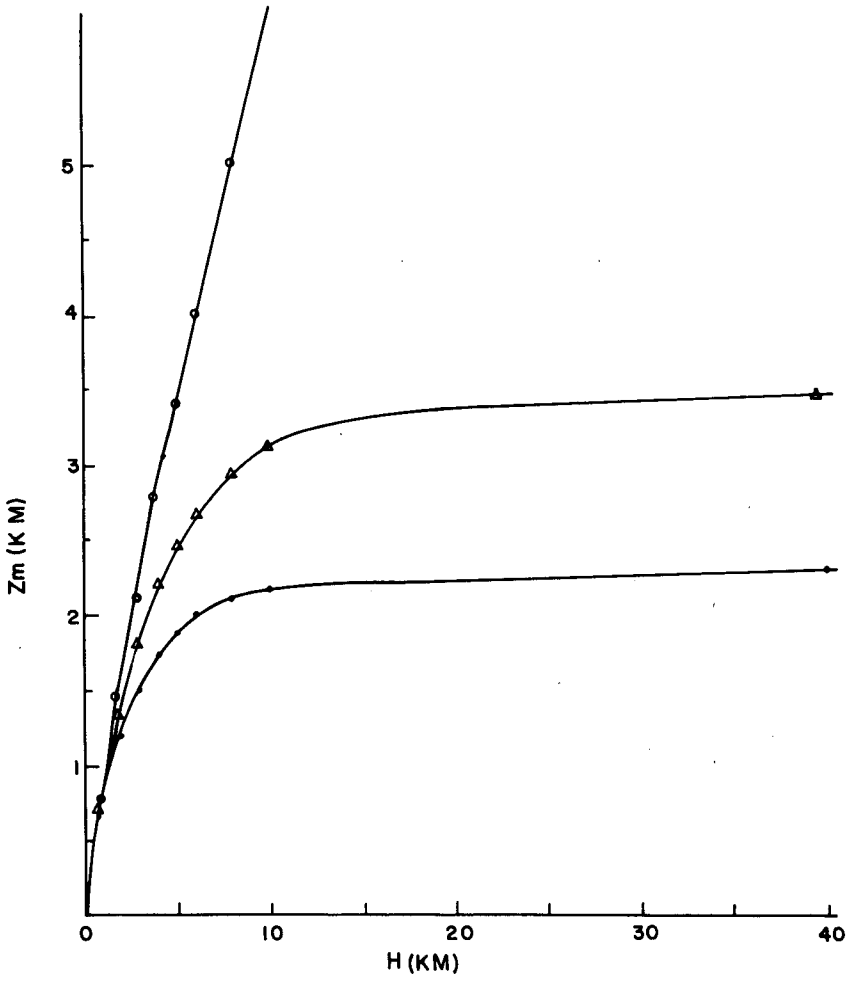

FIG. 2. The elevation of maximum precipitation, z_m, as a function of the bell-shaped mountain height H for three lapse rates: Γ = 2, 6.5 and 10°C km^{-1}. The calculated points are plotted with open circles, triangles and closed circles, respectively.

which reduces to (17) for $\delta = 0$. To solve (31) we have to estimate δ or W_l (if $\bar{u}$ is known). This could be done through the same formula for precipitation when applied to a nearly leveled area upstream whose average precipitation P_0 is given. On substitution of $\partial Z_s/\partial x = 0$ and P_0 into (6) one gets

$$W_l = (P_0 - E)RT(0)/[\epsilon r e_s(0)] \approx P_0 RT(0)/[\epsilon r e_s(0)]. \quad (32)$$

For the Himalayan case where the yearly averaged precipitation P_0 is ~100 cm yr^{-1}, see Dhar and Rakhecha (1980), (32) yields an annual-averaged vertical velocity of $W_l \approx 0.1$ cm s^{-1}.

Equation (31) was numerically solved for different values of W_l. Table 2 summarizes the results for a mountain of H = 5 km and b = 60 km. The lapse rate in these simulations was Γ = 6.5°C km^{-1} and the mean horizontal wind was 5 m s^{-1}.

From Table 2 we learn that within a plausible range of W_l the effect of the synoptic uplift is relatively small. A large increase of W_l yields only a small increase of the point of maximum precipitation, z_m.

3. Theory verification by observations

a. Numerical aspects

In this section, (6) is solved for the precipitation, $P(Z_s)$ as a function of the mountain height, Z_s, at spe-

TABLE 2. The points (x_m, z_m) of maximum precipitation as calculated from (31) for six different values of the large-scale uplift. In this calculation: H = 5 km, b = 60 km, Γ = 6.5°C km^{-1} and $\bar{u}$ = 5 m s^{-1}.

	W_l (cm s^{-1})					
	0	0.1	0.5	1	2	5
x_m	60.6	60.4	59.8	59.1	57.6	53.6
z_m	2.47	2.48	2.51	2.53	2.60	2.78

cific sites where it is assumed that the relative humidity, r, is 1 at all levels; the lapse rate, Γ is 6.5°C km^{-1}; and the large-scale uplift, W_l, is zero. Clearly, the observed x-derivative of the mountain's profile, $\partial Z_s/\partial x$, has strong microscale perturbations (order of less than about 5 km) that we wanted to avoid. This was achieved by a cubic-spline interpolation between the measured points (17 for the Himalayas and Sierra Nevada with a grid distance of $\Delta x \approx 8$ km and 22 points with $\Delta x \approx 14$ km for the Equadorian Andes). Two additional points were added between any two of the aforementioned measured points $Z_s(x_i)$. The derivative $\partial Z_s/\partial x$ was calculated by a centered difference scheme. Negative precipitation values that resulted in negative slopes were set to zero. The model ran in about a third of a second on the CDC 855 at Tel Aviv University.

One of the important processes that was neglected in the formula for precipitation is the advection effect. Clearly, (6) defines a value of precipitation that is solely determined by the local conditions (slope and elevation). In order to account for the precipitation by the upwind clouds that are advected by the horizontal wind $\bar{u}$ the local rainfall value, P_0 was recalculated by

$$P_0 = \frac{1}{W_0} \sum_{i=0}^{N} W_i P_i, \tag{33}$$

where

$$\left.\begin{aligned} W_0 &= \sum_{i=0}^{N} W_i \\ W_i &= \exp[-(x_i - x_0)^2/2\sigma^2] \\ \sigma &= \bar{u} \cdot t, \quad t - \text{time scale} \end{aligned}\right\}.$$

For N we have found that 10 was sufficient for the following experiments, but close to the boundary N was accordingly reduced. According to (33) the precipitation P_0 at any point is determined by the sum of the weighted precipitations upstream. The weight function W_i was chosen to be a normal distribution with a standard devation σ that is proportional to the advective velocity $\bar{u}$ multiplied by the lifetime-scale t of the precipitating cloud. This lifetime was assumed to be half an hour (e.g., see Mason, 1971, p. 282). The Gaussian distribution was preferred since it gives the heavier weight to the neighboring upstream points and a strongly diminished weight to the further points. This is believed to reflect a more realistic situation than, for example, a linear weight function. In any case, the advection was included primarily for smoothing as is discussed later in section 3c.

b. *The Sierra Nevada simulation*

The following simulations are based upon case studies by Colton (1976). He studied the orographically induced precipitation distribution in the central Sierra Nevada Mountains in California, for four fairly strong stormy events. As stated by Colton, the events simulated fit (at least crudely) the criteria that must be met by the model. That is, the synoptic-scale flow pattern is predominantly westerly (at nearly right angles to the mountain barrier) and remains quasi-steady for some period of time.

Clearly, these criteria also meet the demands of our formula for precipitation in its two-dimensional form; see Eq. (6). The inflow profiles of the wind, temperatures and humidities for the initialization of the model were given in Figs. 3 and 4 in Colton (1976, p. 1246). For the application of our formula, the average boundary layer inflow wind $\bar{u}$ was chosen to be the wind intensity at the height of 1000 m. As the lapse rate in all events was approximately 6.5°C km^{-1}, the only additional value we needed was the temperature at the surface, $T(0)$. Table 3 lists the derived values of $\bar{u}$ and $T(0)$ for the four simulations. The dates and periods of the four events are also indicated.

It will be shown later that the model is quite sensitive both to $\bar{u}$ and $T(0)$. The results for simulation 1 from Colton's model and from our formula are shown in Figs. 3a and 3b, respectively. Notice that the dashed line is the model terrain and the solid curve is the model-simulated precipitation rates in Colton (i.e. Fig. 3a), while in Fig. 3b the curve notation is just the opposite. Observed rates during that period for available stations are also plotted on the same figures as given by Colton. The predicted precipitation rates that were calculated by (6) and then "advected" through (33), were multiplied by a constant factor of 0.45 for comparison with the observations. This adjustment factor was kept constant through all the subsequent simulations. We believe that this factor represents the intermittency of the rain-producing processes which leads to a considerable reduction in the average rain intensities when they are averaged over relatively long pe-

TABLE 3. Values of the average horizontal wind, $\bar{u}$, and the surface temperature $T(0)$ that have been used as the input parameters for calculation of the precipitation for the four simulations by Colton (1976). The dates and periods of the simulations are also indicated.

	Simulation			
	1	2	3	4
Date and period	21–22 Dec 1964	21–22 Dec 1955	19–21 Jan 1969	20–21 Dec 1970
$\bar{U}$ (m s^{-1})	20	25	12	11
$T(0)K$	289	288	286	290

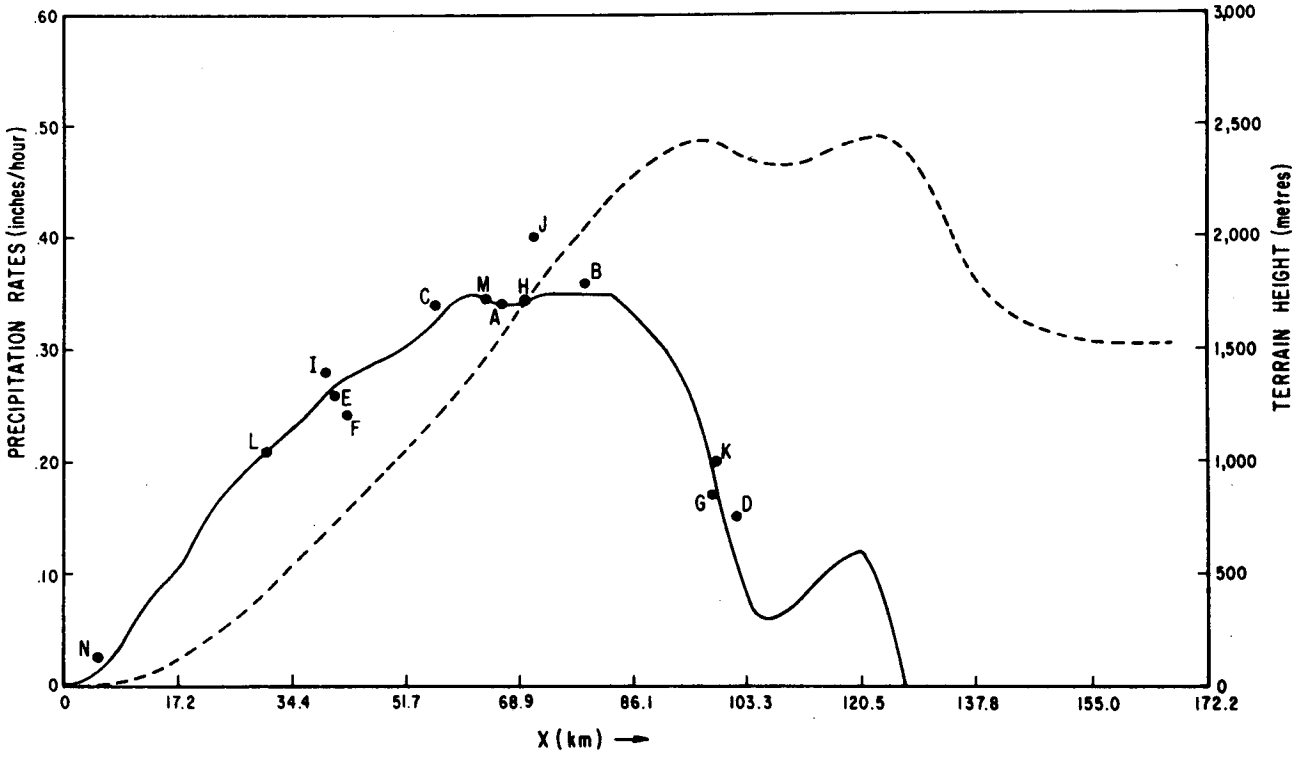

FIG. 3a. From Colton (1976, Fig. 7). Model simulated rates (solid curve) for simulation 1. Observed rates are plotted as dots. Letters near dots identify the observing station. The latter are listed in Colton (1976, Table 1). Dashed line is the model terrain of the Sierra Nevada mountains.

riods as compared, for example, with the lifetime of a cloud. Figures 3a and 3b illustrate that the region of heaviest precipitation is almost correctly positioned. The height of maximum precipitation z_m is about 1.8 km, both in the model and observations. The sharp decrease at the lee of the mountain (points K, G and D) is also well simulated. But contrary to Colton's result, the downhill precipitation is larger in our prediction as compared to the observations, i.e., points L, I, E and F. Keeping in mind that our results are based on a very simple formula, which totally neglects the evolving dynamics of the flow over the mountain and the detailed vertical profiles of the inflow, it is rather surprising to find that the above formula succeeds in predicting the basic features of the distribution.

In the second simulation, Figs. 4a and 4b, the average wind is stronger and there is an increase in the amount of precipitation. The elevation of maximum precipitation z_m raises to about 1.9–2 km in accordance with the observations. Again, there are excessive precipitation rates which are particularly noticed in our prediction (see points E, O, F, Q in Fig. 4b). Figures 5a and 5b show the results for the third simulation. The precipitation rates are considerably less here than during the previous two simulations. The overall precipitation simulation is in reasonably good agreement with the observations. In the fourth simulation, indicated in Figs. 6a and 6b, the precipitation rates are slightly higher than those for the previous event, but the Colton model results, as well as our results, underestimate this increase of rainfall. It is interesting to notice that the basic deficiencies as well as the basic prediction abilities emerge in our prediction as in the Colton model results. This relatively large success of the precipitation formula

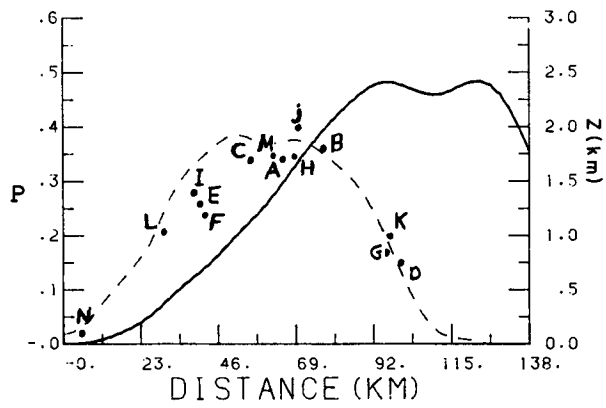

FIG. 3b. The precipitation rates in inches/hour by (6) and (33) for the first simulation. Dashed line is for precipitation and solid line is for the model terrain. Observed rates are plotted as in Fig. 3(a) by dots.

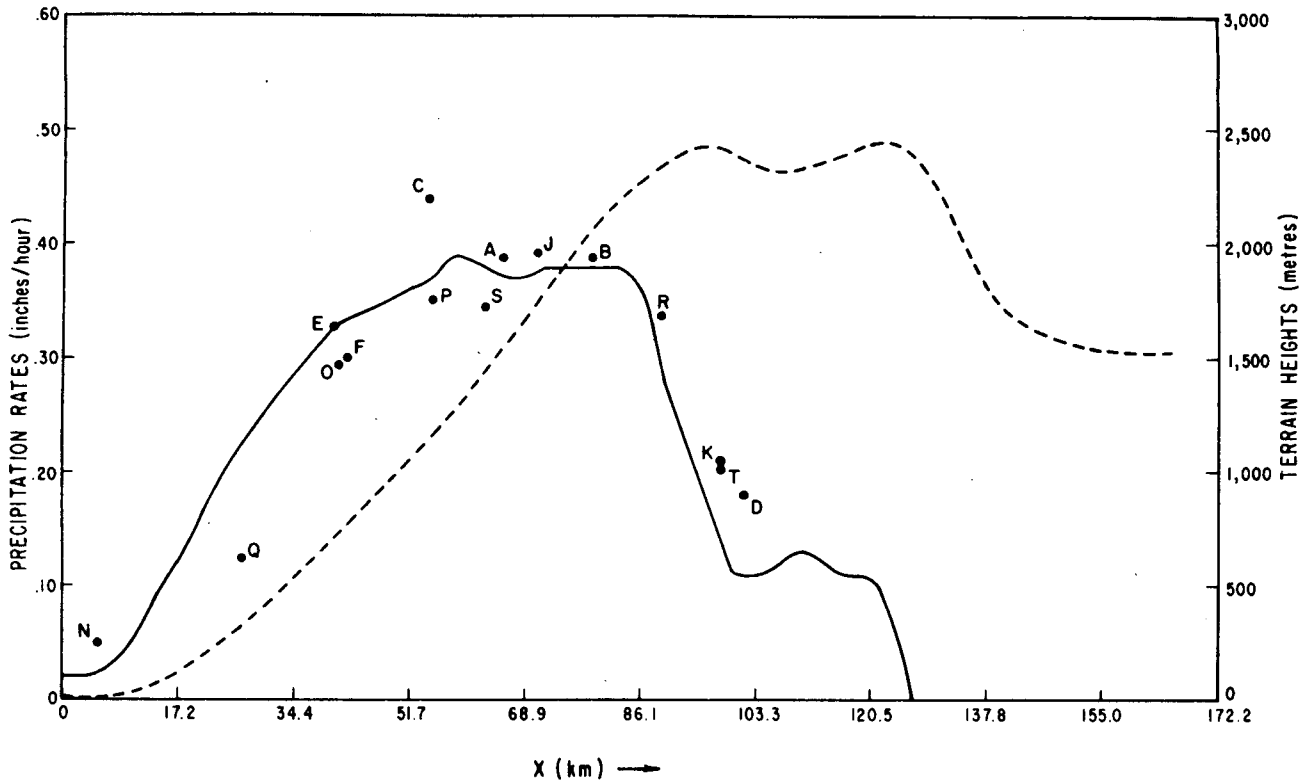

FIG. 4a. As in Fig. 3(a) but for simulation 2.

was unexpected, and is attributed to the fact that the basic physical processes were fairly well approximated. In particular, the slope-induced vertical velocities and the reduction in moisture availability with height due to the cooler air above seem to represent the two basic physical factors that dominate the distribution of precipitation over high mountains.

Before turning to the next simulation we would like to point out the large effect of the surface temperature $T(0)$, on the amounts of precipitation. Figure 7 repeats the third simulation but with surface temperature increased by 4 K. Instead of $T(0) = 286$ K the input is 290 K; the same temperature as in the *fourth* simulation. As is expected, the precipitation rates are significantly higher with the higher temperatures. This explains the higher precipitation in the fourth simulation relative to the third one, although the horizontal velocity $\bar{u}$ is even slightly lower in the fourth simulation. It is the Clausius-Clapeyron equation that determines the increased ratio of the precipitation. If the temperature T increases by ΔT, the ratio of the enhanced precipitation P_2, to the precipitation with the temperature T, P_1, may be approximated by,

$$P_2/P_1 \approx \exp\left[\frac{L_c}{R_v T(0)} \cdot \frac{\Delta T}{T}\right]. \qquad (34)$$

On the substitution of the values $\Delta T = 4$ K, $T = 300$ K, $L_c/(R_v T(0)) \approx 19$, one finds this ratio to be 1.28. This ratio is in accordance with the precipitation rates presented by Fig. 7.

c. *The Himalayan simulation*

Dhar and Rakhecha (1980) studied the relationships between the mean monsoon rainfall and the elevation in the central Himalayan region. They have shown several important features. First, that a linear relationship between elevation and monsoon rainfall does not exist. Also, elevation and rainfall can best be related

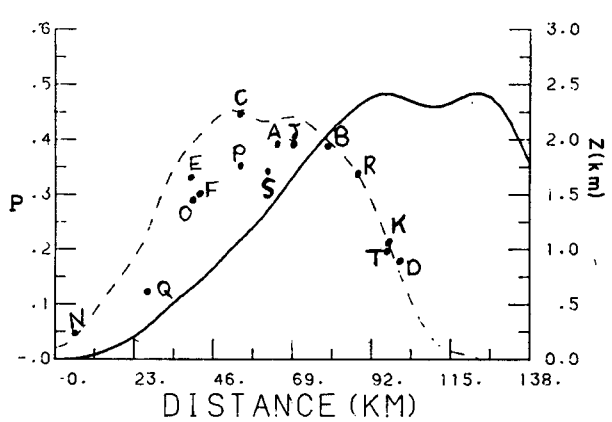

FIG. 4b. As in Fig. 3(b) but for simulation 2.

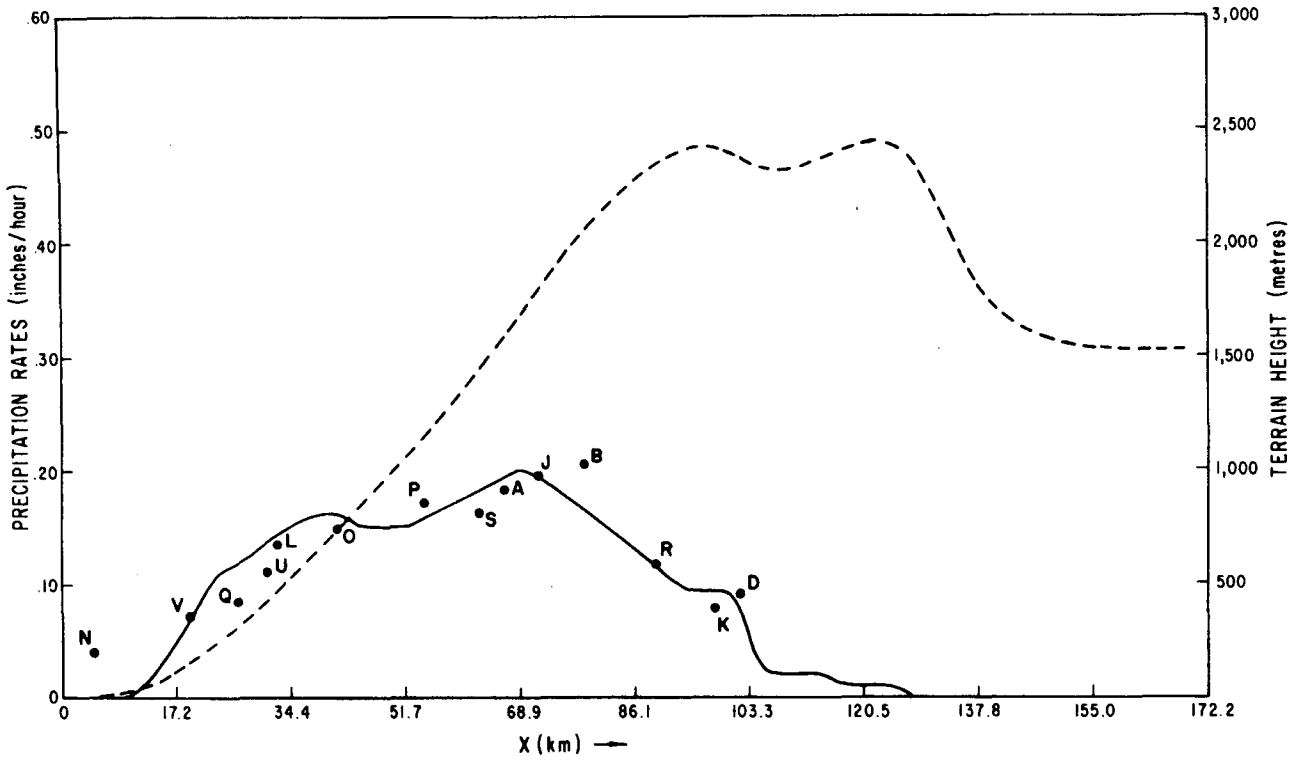

FIG. 5a. As in Fig. 3(a) but for simulation 3.

by a polynomial of the fourth degree, and that rainfall–elevation profiles show two zones of maximum rainfall, one near the foothills and the other at an elevation of 2.0–2.4 km. The mean elevation profiles of precipitation for two cross-sections of the Himalayas are shown in Fig. 8, which is Fig. 16.4 in Dhar and Rakhecha (1980, p. 260). The figures clearly show the three major parallel ranges of the Himalayas: the Siwalik, the Lesser and the Great Himalayas. The data is based upon about 50 rainfall stations. Only four of the stations were located above the elevation of 2500 meters.

The curves presented by Fig. 8 indicate the two zones of maximum rainfall—at the foothills and at an elevation of 2.0–2.4 km. The first zone of *minimum* rainfall is located at an elevation of about 0.6–0.8 km. Figure 9a depicts the predicted distribution of the normalized precipitation according to (6) and (33). The ground profile of the western cross section of the Himalayas (Kosi West) was chosen for the simulation. Based upon the average monsoonal wind data by Findlater (1980), for the height of 1 km, we assumed $\bar{u} \approx 10$ m s^{-1}. The surface temperature at the sea level height $T(0)$ was 300 K, while the other parameters were left as in the previous experiments. If one neglects the secondary minima at about 1.6 km, one finds that the locations of the first two maxima agree with the observations. One is at the foothills of the Himalayas and the other maxima is at the elevation of 1.5–2.2 km depending on the way in which the smoothing of the secondary minima is performed (see the resulting dotted line in Fig. 9a). The first minima of precipitation is predicted at the height of about 0.55 km and this is in agreement with the elevation of the observed minima—0.6 to 0.8 km. The maximum precipitation rate near the origin is the result of the steep slope right at the foothills, as may be noticed in Fig. 8.

The most interesting result of the rainfall distribution is the third maxima, at the elevation of about 4 km. This maxima, if it exists, couldn't be observed because no rainfall stations were located at the Great Himalayan range at elevations above 3200 m. This unobserved

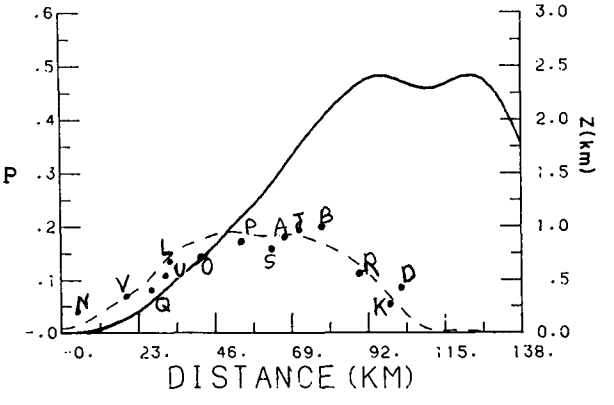

FIG. 5b. As in Fig. 3(b) but for simulation 3.

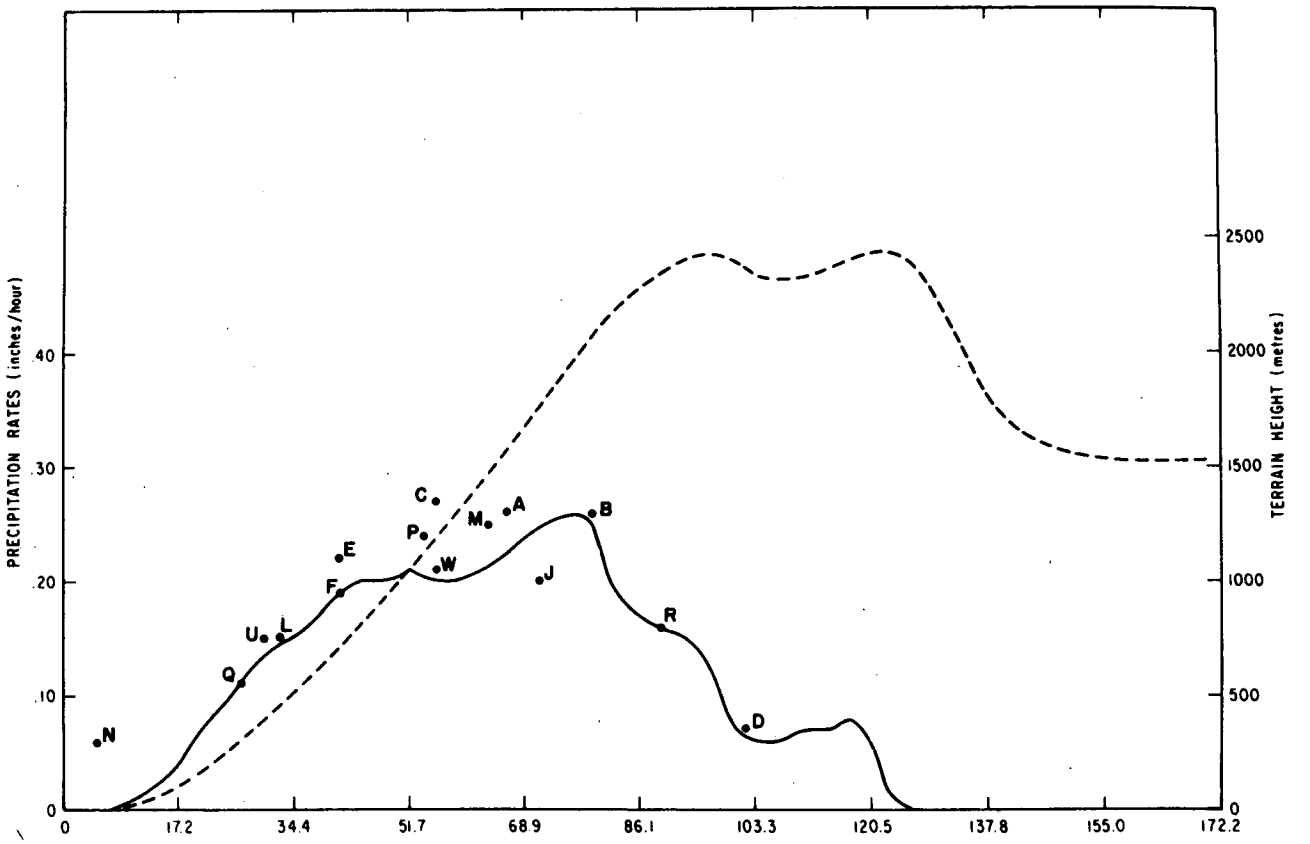

FIG. 6a. As in Fig. 3(a) but for simulation 4.

maximum is weaker in relation to the other maxima. But, even the increase of precipitation toward this maxima at elevations above 2.2 km (over the great Himalayan Range) is impossible to detect in the observations, as only few stations were reporting above that level of 2.2 km. The answer to the question of whether such a maximum really exists depends crucially upon the temperature and moisture profiles. The assumption of a saturated troposphere (i.e., $r = 1$), which is realistic through the precipitating lower troposphere above the mountain, may not be quite so when reaching the higher levels. Following our estimation of $\max(z_m)$ for the bell-shaped mountain by (27), the elevation of maximum precipitation (i.e., z_m) cannot exceed the moisture scale height, h_q. Taking $h_q \approx 4$ km, we conclude that the third maxima over the

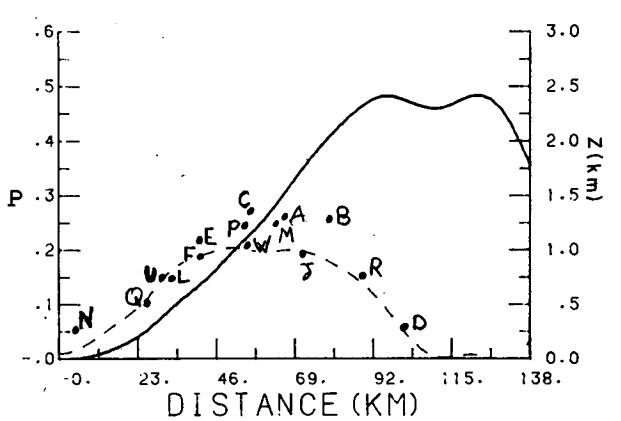

FIG. 6b. As in Fig. 3(b) but for simulation 4.

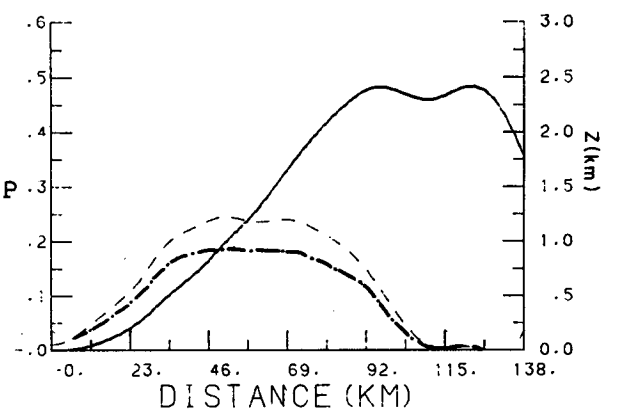

FIG. 7. As in Fig. 5(b) but with an additional dashed line for the precipitation rates where the surface temperature $T(0)$ is equal 290° K. The dashed-dotted line is for $T(0) = 286$°K.

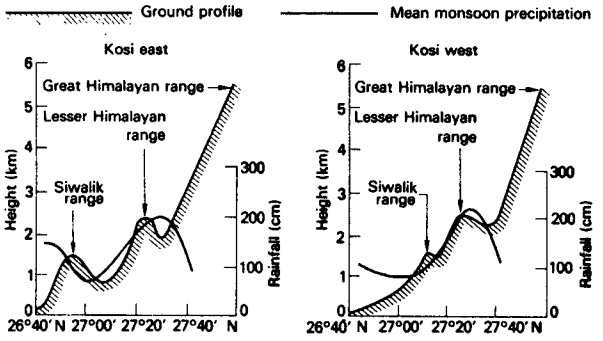

FIG. 8. From Dhar and Rakhecha (1980, Fig. 16.4). A schematic representation of the mean monsoon precipitation across the Kosi Himalayas.

Himalayas (at $Z_s \approx 4$ km) is just about at the upper realistic limit for the maximum precipitation. Therefore, if such a maximum exists its intensity might be even weaker than that predicted by Fig. 9a.

Figure 9b repeats the Himalayan experiment with a reduced horizontal wind of $\bar{u} \approx 5$ m s^{-1}. Consequently the absolute precipitation rates are reduced by half but the changes we may notice in the *normalized* precipitation values are solely due to the weaker advection [see (33)]. The minima and maxima points are more pronounced and somewhat shifted to the west (i.e., toward lower elevations). A similar result could also be obtained by cutting the time scale of the precipitating cloud by half, to 900 s. In both cases the advection process is reduced due to the smaller standard deviation σ of the weight function. The effect of enhancing the advection is illustrated in Fig. 9c where the lifetime t of the precipitating cloud is doubled to one hour. The precipitation profile is strongly smoothed, as is noticed by the reduction in the extreme points on the curve. Figures 9a–c illustrate the advection effects, from which the most prominent is the smoothing of the curve. The result of completely ignoring the advection enhances the extrema. For example, the negative slopes yield zero precipitation even though the upstream neighboring points may attain high rainfall intensities. Ev-

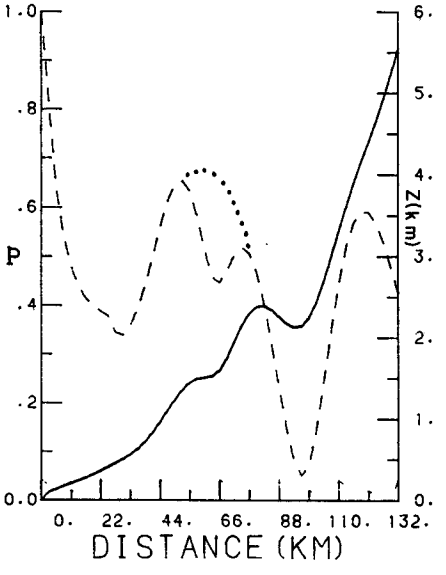

FIG. 9a. The normalized precipitation rates (dashed line) over the Himalayas. Kosi West, by (6) and (33). The solid line is the model terrain, see Fig. 8. The horizontal wind $\bar{u} = 10$ m s^{-1}. For the other parameters see text. The dotted curve indicates the approximation for comparison with the observations. Location of extrema above the mountain is found by following the extreme ordinate to the model terrain and then refer to the mountain height on the right scale.

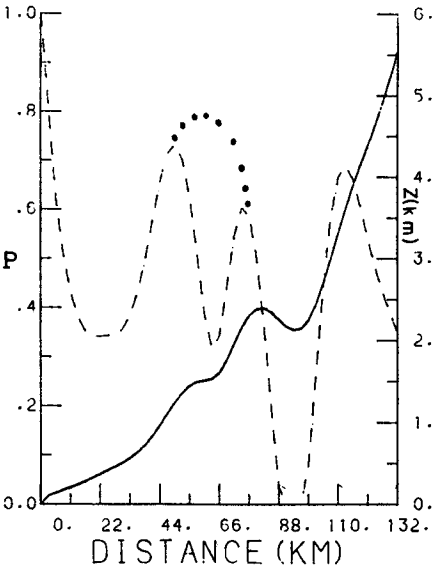

FIG. 9b. As Fig. 9(a) except for $\bar{u} = 5$ m s^{-1}.

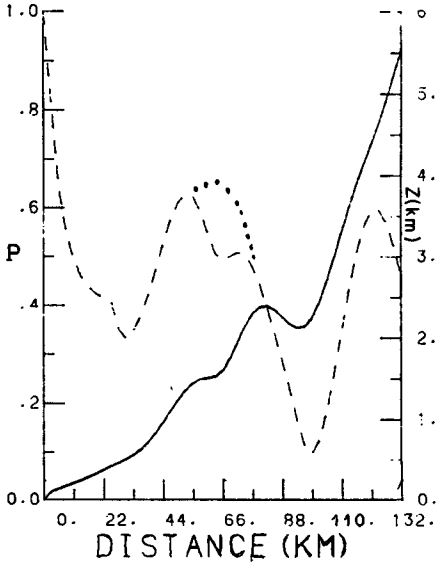

FIG. 9c. Same as Fig. 9(a) except for $t = 3600$ s.

idently, the inclusion of advection prevents such a situation and does so in a physically meaningful manner. This is not, however, fulfilled in Fig. 9b where the precipitation goes to zero at near 88 km, because of the weaker advective effect as compared to the cases in Figs. 9a and 9c.

d. The Andes simulation

We have also simulated the distribution of annual precipitation over the Equadorian Andes based upon cross sections and precipitation data from Rumley (1965). Figure 10 presents the predicted normalized annual precipitation for Rumley's cross section 4 from Manta to Puyo, Equador. The main maxima indicated by this study is at approximately 2.7 km but only the secondary maxima at about 1 km was detected by Rumley (1965). Again, as in the Himalayas the predicted maxima at near 195 km (height of ~2.7 km) is impossible to detect in the observations due to lack of high elevation data. It is impossible to do any beneficial comparison with the observations as only one or two stations were available above the main slope for each of the cross sections being discussed by Rumley. The normalized observed precipitation at the four points reported by Rumley are also indicated in Fig. 10. The precipitation values given by Rumley were normalized by the maximum of 3344 mm. The fit to the data is rather poor for this case and it is believed to be the result of the major *nonorographic* contribution to the precipitation at the pertinent stations (e.g., see stations 10, 11 and even 12 in Fig. 10).

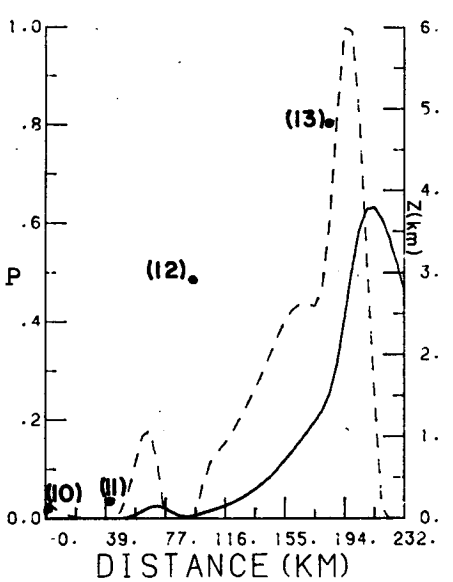

FIG. 10. Normalized precipitation (dashed line) over the Andes. The solid line is a cross section of the Andes from Manta to Puyo in Equador. The observed normalized rates at four points are indicated by the numbers 10 to 13. Data for the cross section and precipitation is according to Rumley (1965, p. 46).

4. Summary and conclusions

The main conclusion from this study is that the distribution of orographic precipitation over mountains could be well approximated by the convergence of moisture through the boundary layer

$$\bar{\rho}\bar{q}\cdot(-\overline{\nabla_H\cdot\mathbf{V}})H_0,$$

where this convergence is derived from the local slope. The simulated distributions of the precipitation over mountains were compared with observations and were found in good agreement both on the basis of annual averages and on the basis of single storms. The latter results are for the four simulations that were reported by Colton (1976) over the Sierra Nevada Mountains in California, i.e., comparable results were obtained to those from a numerical model employing seven conservation equations. The fairly good agreement suggests that the most important physical factors in determining the rainfall distribution are the reduction in moisture availability at higher altitudes due to the cooler air and the water vapor convergence induced by the local slope. However, we had to introduce a constant scale factor of 0.45 for comparison with the actual precipitation rates. This was not unexpected because one of our model's basic assumptions is a precipitation efficiency of 100 percent, which is at least three to four times larger than the realistic value (see, e.g., Rogers, 1976, stating the value of 19%). The contribution to the rainfall rate distribution by evaporation was found to be very minor.

Items of note from analyses performed include that for a bell-shaped mountain, the elevation of maximum precipitation z_m is determined mainly by the atmospheric lapse rate and the height of the mountain. As the lapse-rate increases, z_m decreases. The maximum precipitation rate is in general shifted downward from the point with the steepest slope. The higher the mountain, the higher the elevation of maximum precipitation, unless the aspect ratio H/b is kept constant, in which case z_m does not change.

Another interesting result is the existence of an upper limit for the elevation of maximum precipitation in the nonisothermic atmosphere. Given the assumptions employed herein, this upper limit, $\max(z_m)$, is independent of the slope, or of the height of the mountain, and for a saturated atmosphere with a realistic lapse-rate of $\Gamma_s = 6.5°\text{C km}^{-1}$, the value of this upper limit is given by ~3.8 km. In the case where the specific humidity could be assumed constant through the boundary layer and is reduced above it through a lapse rate Γ_q, one finds that $\max(z_m)$ is determined by the smallest of the moisture scale height and the tropospheric scale height. The effect of a constant large-scale uplifting W_l, on the elevation of maximum precipitation was found small.

The model appears to yield useful results for the distribution of precipitation rate over mountains. It is

possible that particularly for *high* mountains the detailed microphysical processes are less essential for realistically modeling the precipitation distributions, (strictly speaking the model supplies us with the precipitation *rate* distributions, but they are approximately the orographic precipitation distribution). It seems that for small or medium size hills this is not as much so, and both microphysical processes as well as the detailed mesoscale flow play a more significant role as discussed by Browning (1980). The rainfall rate distribution was found quite sensitive to the horizontal wind intensity, surface temperature, temperature lapse rate, and the specific humidity lapse rate.

Acknowledgments. I wish to thank Prof. R. S. Lindzen for introducing me to some of the problems in tropical meteorology. Many thanks also go to Prof. Z. Levin for helpful comments. Thanks to the reviewers for their helpful comments. A special thanks to Ms. Rachel Duani for the nice typing of the manuscript.

REFERENCES

Augstein, E., H. Schmidt and F. Ostapoff, 1974: The vertical structure of the atmospheric boundary layer in undisturbed trade winds over the Atlantic Ocean. *Bound. Layer Meteor.*, **6**, 129–150.

Browning, K. A., 1980: Structure, mechanism and prediction of orographically enhanced rain in Britain. GARP Publ. Ser. No. 23, WMO, 85–114.

Burns, J. I., 1953: Small-scale topographic effects on precipitation distribution in San Dimas experimental forest. *Trans. Amer. Geophys. Union*, **34**, 761–768.

Cho, H. R., and Y. Ogura, 1974: A relationship between cloud activity and the low-level convergence as observed in Reed–Recker's composite easterly waves. *J. Atmos. Sci.*, **31**, 2058–2065.

Colton, D. E., 1976: Numerical simulation of the orographically induced precipitation distribution for use in hydrologic analysis. *J. Appl. Meteor.*, **15**, 1241–1251.

Dhar, O. N., and P. R. Rakhecha, 1980: The effect of elevation on monsoon rainfall distribution in the Central Himalayas. *Monsoon Dynamics.* J. Lighthill, and R. P. Pearce, Eds., Cambridge University Press, 253–260.

Donley, D. E., and R. L. Mitchell, 1939: The relation of rainfall to elevation in the Southern Appalachian region. *Trans. Amer. Geophys. Union.*, **20**, 711–721.

Findlater, J., 1981: An experiment in monitoring cross–equatorial airflow at low level over Kenya and rainfall of western India during the northern summers. *Monsoon Dynamics.* J. Lighthill and R. P. Pearce, Eds., Cambridge University Press, 309–319.

GATE, 1980: *Proc. of the NAS Symp. on the Impact of GATE on Large-Scale Numerical Modelling of the Atmosphere and Ocean.* Woods Hole Oceanographic Institution, 1979.

Haltiner, G. J., and R. T. Williams, 1980: *Numerical Prediction and Dynamic Meteorology.* Wiley & Sons, 477 pp.

Hess, S. C., 1959: *Introduction to Theoretical Meteorology.* Holt, 362 pp.

Linsley, R. K., M. A. Kohler and J. L. H. Paulhus, 1958: *Hydrology for Engineers,* McGraw–Hill, 340 pp.

Mason, B. J., 1971: *The Physics of Clouds,* 2nd Ed., Clarendon Press, 671 pp.

Ramage, C. S., F. R. Miller and C. Jefferies, 1972: *Meteorological Atlas of the Indian Ocean Expedition,* Vol. 1. *The Surface Climate of 1963 and 1964.* Natl. Sci. Found., Washington, DC.

Rodda, J. C., 1951: An objective method for the assessment of areal rainfall amounts. *Weather*, **17**, 54–59.

Rogers, R. R., 1976: *A Short Course in Cloud Physics,* Pergamon, 227 pp.

Rumley, G. B., 1965: An investigation of the distribution of rainfall with elevation for selected stations in Equador. M.S. thesis, Texas A&M University, 66 pp.

Spreen, W. C., 1947: Determination of the effect of topography upon precipitation. *Trans. Am. Geophys. Union*, **28**, 285–290.

Stevens, D. E., and R. S. Lindzen, 1978: Tropical wave–CISK with a moisture budget and cumulus friction. *J. Atmos. Sci.*, **35**, 940–961.

Stidd, C. K., and L. B. Leopold, 1951: The geographical distribution of average monthly rainfall, Hawaii. *Meteor. Monogr.*, **1**, 24–33.